Spin-orbit coupled systems in the atomic limit: rhenates, osmates, iridates

Arun Paramekanti, David J. Singh, Bo Yuan, Diego Casa, Ayman Said, Young-June Kim, and A. D. Christianson

Phys. Rev. B **97**, 235119 — Published 11 June 2018

DOI: 10.1103/PhysRevB.97.235119

Spin-orbit coupled systems in the "atomic" limit: rhenates, osmates, iridates

Arun Paramekanti,[1,2] David J. Singh,[3] Bo Yuan,[1] Diego Casa,[4] Young-June Kim,[1] and A. D. Christianson[5,6,7]

[1] *Department of Physics, University of Toronto, Toronto, Ontario M5S 1A7, Canada*
[2] *Canadian Institute for Advanced Research, Toronto, Ontario, M5G 1Z8, Canada**
[3] *Department of Physics and Astronomy, University of Missouri, Columbia, Missouri 65211-7010, USA†*
[4] *Advanced Photon Source, Argonne National Laboratory, Argonne, Illinois 60439, USA*
[5] *Materials Science & Technology Division, Oak Ridge National Laboratory, Oak Ridge, TN-37831, USA*
[6] *Neutron Scattering Division, Oak Ridge National Laboratory, Oak Ridge, TN-37831, USA*
[7] *Department of Physics & Astronomy, University of Tennessee, Knoxville, TN-37966, USA*

(Dated: June 1, 2018)

Motivated by RIXS experiments on a wide range of complex heavy oxides, including rhenates, osmates, and iridates, we discuss the theory of RIXS for site-localized t_{2g} orbital systems with strong spin-orbit coupling. For such systems, we present exact diagonalization results for the spectrum at different electron fillings, showing that it accesses "single-particle" and "multi-particle" excitations. This leads to a simple picture for the energies and intensities of the RIXS spectra in Mott insulators such as double perovskites which feature highly localized electrons, and yields estimates of the spin-orbit coupling and Hund's coupling in correlated $5d$ oxides. We present new higher resolution RIXS data at the Re-L_3 edge in Ba_2YReO_6 which finds a previously unresolved peak splitting, providing further confirmation of our theoretical predictions. Using *ab initio* electronic structure calculations on $Ba_2\mathcal{M}ReO_6$ (with $\mathcal{M}$=Re, Os, Ir) we show that while the atomic limit yields a reasonable effective Hamiltonian description of the experimental observations, effects such as t_{2g}-e_g interactions and hybridization with oxygen are important. Our *ab initio* estimate for the strength of the intersite exchange coupling shows that, compared to the d^3 systems, the exchange is one or two orders of magnitude weaker in the d^2 and d^4 materials, which may partly explain the suppression of long-range magnetic order in the latter compounds. As a way to interpolate between the site-localized picture and our electronic structure band calculations, we discuss the spin-orbital levels of the $\mathcal{M}O_6$ cluster. This suggests a possible role for intracluster excitons in Ba_2YIrO_6 which may lead to a weak breakdown of the atomic $J_{\rm eff} = 0$ picture and to small magnetic moments.

I. INTRODUCTION

In recent years, much attention has been paid to complex oxides of heavy transition elements where electronic correlations become comparable to the spin-orbit coupling (SOC) λ. This provides a new route to realizing exotic quantum ground states.[1] A large part of this effort has been focussed on the Ir^{4+} iridates with a $5d^5$ configuration, corresponding to a single hole in the t_{2g} orbitals.[2–8] At this filling, the physics is that of a half-filled $j_{\rm eff} = 1/2$ band, with the total angular momentum $j_{\rm eff}$ arising from the coupling of the spin to the effective orbital angular momentum $\ell_{\rm eff} = 1$ of the t_{2g} triplet. Interest in the spin-orbit coupled materials stems from the possibility of realizing analogues of high-temperature superconductivity upon electron doping, and exotic magnetic phases such as Kitaev spin liquids and topological semimetals.[9–19] Currently, there is an effort to explore other complex oxides, such as osmates and rhenates, as well as iridates with different valence states, which may lead to further exotic phenomena at different electron fillings.[20–28] An important step in this programme is to elucidate the 'atomic' interactions which govern the local physics, which then feeds into understanding how such local degrees of freedom interact and organize at longer length scales. Here, we discuss this step in the context of double perovskite materials using a theoretical analysis of resonant inelastic X-ray scattering (RIXS), exact diagonalization studies of the single-site problem with SOC at different electron fillings (d^2, d^3, d^4), and complementary *ab initio* electronic structure calculations.[?]

RIXS has proven to be a particularly valuable tool to explore spin and orbital excitations, and there has been extensive experimental[29–36] and theoretical work[37–51] in this area (see Ref. 52 for a review). In this paper, we discuss the theory of RIXS for systems with highly localized t_{2g} electronic states at various fillings. Using exact diagonalization (ED) calculations of the RIXS spectrum, we show that we can quantitatively extract the spin-orbit and Hund's couplings, and explain both the energies and the spectral intensities observed in experiments on rhenates, osmates, and iridates. We also present new experimental high resolution RIXS results on Ba_2YReO_6 at the Re L_3 edge which finds a peak splitting in the spectrum, in perfect agreement with our theoretical predictions. This splitting was not resolved in previous experiments at the Re L_2 edge. This paper thus extends and generalizes previous well-known work on RIXS for $5d^5$ iridates,[43] and provides a useful companion to a recent study of the RIXS operator in t_{2g} spin-orbital systems.[53]

Additionally, in order to complement this effective Hamiltonian study, we have carried out *ab initio* electronic structure calculations for the cubic double perovskites Ba_2YReO_6, Ba_2YOsO_6, and Ba_2YIrO_6. This permits us to understand material-to-material variations of these effective parameters across the $5d$ oxides, and to show that t_{2g}-e_g interactions and hybridization with the ligand ions (oxygen) play a key role when we attempt to

connect the parameters of the effective Hamiltonian with a more microscopic theory. Furthermore, our *ab initio* estimates for the strength of the magnetic exchange coupling between moments in these materials shows that, compared to the osmates, the exchange is one or two orders of magnitude weaker in the rhenates and iridates. This could explain the robust magnetic long range order observed in the osmates, which should be contrasted with weak ordering tendencies in the latter compounds.

Based on our *ab initio* calculations, hybridization of the transition metal ion with the surrounding oxygen octahedral cage plays an important role in complex $5d$ oxides. This leads us to examine the spin-orbital states on the $\mathcal{M}O_6$ metal-oxygen octahedra, which could be useful in future studies of the effect of extended interactions on such clusters as a way to bridge the gap between ED and DFT results on Ba_2YIrO_6.

II. RIXS FOR HIGHLY LOCALIZED STATES

The Kramers-Heisenberg expression[37–41,52] for the two-photon RIXS scattering cross section is given by

$$\frac{d^2\sigma}{d\Omega dE_{\rm in}} = \frac{E_{\rm out}}{E_{\rm in}} \sum_f \left| \sum_n \frac{\langle f|T^\dagger|n\rangle\langle n|T|g\rangle}{E_g - E_n + E_{\rm in} + i\frac{\Gamma_n}{2}} \right|^2 \times \delta(E_g - E_f + E_{\rm in} - E_{\rm out}). \quad (1)$$

Here, g, n, f refer to ground (initial) state, intermediate state, and final state, respectively with corresponding energies E_g, E_n, E_f, and Γ_n is the inverse lifetime of the intermediate state. $E_{\rm in} = \hbar\omega_{\rm in}$ and $E_{\rm out} = \hbar\omega_{\rm out}$ are the incoming and outgoing photon energies, and the δ-function enforces energy conservation. Within the dipole approximation for the photon field, the transition is induced by the dipole operator $T \sim \hat{\epsilon}\cdot\mathbf{r}$, where $\hat{\epsilon}$ denotes the photon polarization, which we label as $\hat{\epsilon}_{\rm in}$ for the incoming photon which excites from the ground state (which enters in the $\langle n|T|g\rangle$ matrix element above), and $\hat{\epsilon}_{\rm out}$ for the outgoing photon which de-excites into the final state (which enters in the $\langle f|T^\dagger|n\rangle$ matrix element above). On resonance, with $E_{\rm out} \approx E_{\rm in}$ (since the energy transfer $E_f - E_g \ll E_{\rm in}, E_{\rm out}$), the cross section simplifies to

$$\frac{d^2\sigma}{d\Omega dE_{\rm in}} \approx \frac{1}{A} \sum_f \left| \sum_n \langle f|T^\dagger|n\rangle\langle n|T|g\rangle \right|^2 \times \delta(E_g - E_f + E_{\rm in} - E_{\rm out}) \quad (2)$$

where the prefactor $A = \left| E_g - \bar{E}_n + E_{\rm in} + i\frac{\bar{\Gamma}_n}{2} \right|^2$, with $\bar{E}_n, \bar{\Gamma}_n$ being the *average* energy and inverse lifetime of the intermediate states. This approximation, which is valid for short core-hole lifetime,[38,39] allows us to ignore intermediate state interactions between the core-hole and other electrons. We show below that the resulting spectra are in good agreement with experiments, providing a phenomenological justification for this approximation.

RIXS excites an electron from a highly spin-orbit coupled core level into the relevant d-orbitals; here, we focus on excitation into the t_{2g} states. This leads to an intermediate state with a core-hole and an added electron in the t_{2g} orbitals. These intermediate states decay on the timescale of the core-hole lifetime $\sim 1/\Gamma_n$, leaving the original t_{2g} electrons in a final excited spin-orbital state. We can thus consider simplified transition matrix elements[24]

$$\langle n|T|g\rangle = \hat{\epsilon}^\alpha_{\rm in}\langle n|p^\dagger_{\beta\sigma}d^\dagger_{\alpha\beta\sigma}|g\rangle \quad (3)$$

$$\langle f|T^\dagger|n\rangle = \hat{\epsilon}^\mu_{\rm out}\langle f|d_{\mu\nu\sigma'}p_{\nu\sigma'}|n\rangle. \quad (4)$$

Here $p^\dagger_{\alpha\sigma}$ creates a $2P$ core-hole in orbital α ($\alpha = p_x, p_y, p_z$) with spin σ, while $d^\dagger_{\alpha\beta\sigma}$ creates a d-electron in the t_{2g} orbital (d_{yz}, d_{zx}, d_{xy}) with spin σ, and we have restricted attention to parity-allowed nonzero dipole matrix elements. Using this, we arrive at the following expression for the RIXS cross-section:

$$\frac{d^2\sigma}{d\Omega dE_{\rm in}} \propto \sum_f \left| \sum_n \hat{\epsilon}^\mu_{\rm out}\hat{\epsilon}^\alpha_{\rm in}\langle f|d_{\mu\nu\sigma'}p_{\nu\sigma'}|n\rangle\langle n|p^\dagger_{\beta\sigma}d^\dagger_{\alpha\beta\sigma}|g\rangle \right|^2 \times \delta(E_g - E_f + E_{\rm in} - E_{\rm out}). \quad (5)$$

The core-level part of the process consists of exciting a single core-hole from the core-vacuum and de-exciting back into the vacuum, with intermediate states for the core-hole being $2P_{1/2}$ (L_2 edge) or $2P_{3/2}$ (L_3 edge). Let us denote the corresponding P-matrix elements as $M^J_{\nu\sigma';\beta\sigma}$ with $J = 1/2, 3/2$. This leads to $(d^2\sigma/d\Omega dE_{\rm in}) \propto \mathcal{I}_J(\omega)$, where

$$\mathcal{I}_J(\omega) \equiv \sum_f \left| \sum_n \hat{\epsilon}^\mu_{\rm out}\hat{\epsilon}^\alpha_{\rm in}M^J_{\nu\sigma';\beta\sigma}\langle f|d_{\mu\nu\sigma'}|n\rangle\langle n|d^\dagger_{\alpha\beta\sigma}|g\rangle \right|^2 \times \delta(E_g - E_f + \hbar\omega), \quad (6)$$

with $\hbar\omega = E_{\rm in} - E_{\rm out}$ being the photon energy loss. We continue to use the notation g, n, f, for ground, intermediate, and final states, but henceforth these will refer to only the t_{2g} states.

The matrix M^J for the core hole for the L_2 and L_3 edges is given by

$$M^{J=1/2} = \frac{1}{3}(1 - \vec{L}\cdot\vec{S}) \quad (7)$$

$$M^{J=3/2} = \frac{1}{3}(2 + \vec{L}\cdot\vec{S}) \quad (8)$$

where L, S refer to the oxygen $2P$ hole orbital- and spin angular momentum operators. Labelling the P-states as $(\mu\sigma) = (p_x\uparrow, p_y\uparrow, p_z\uparrow, p_x\downarrow, p_y\downarrow, p_z\downarrow)$, we can explicitly write out

$$M^{J=1/2} = \frac{1}{3}\begin{pmatrix} 1 & -i & 0 & 0 & 0 & -1 \\ i & 1 & 0 & 0 & 0 & -i \\ 0 & 0 & 1 & 1 & i & 0 \\ 0 & 0 & 1 & 1 & i & 0 \\ 0 & 0 & -i & -i & 1 & 0 \\ -1 & i & 0 & 0 & 0 & 1 \end{pmatrix} \quad (9)$$

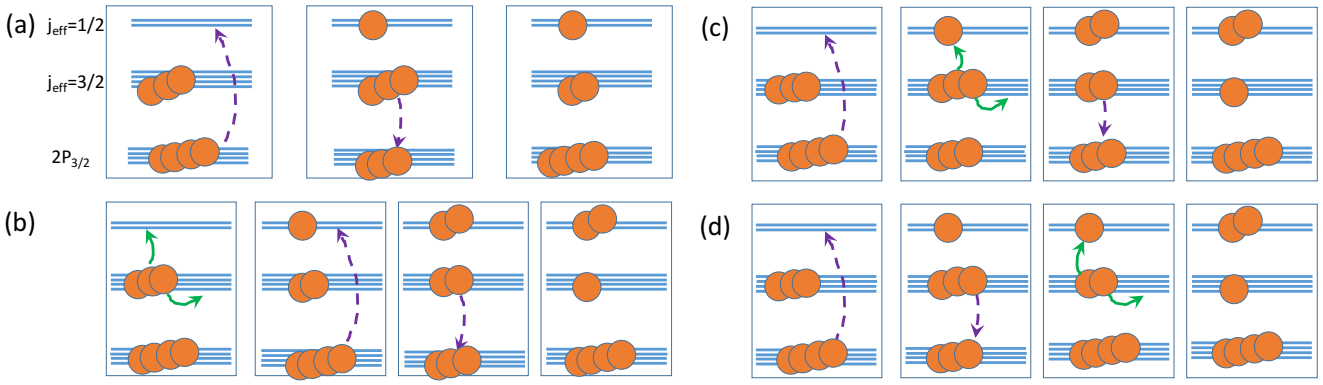

FIG. 1. (Color online) Schematic picture of the L_3 edge inelastic RIXS processes (for the $5d^3$ osmates), with dashed (purple) lines indicating photon-induced transitions and solid (green) lines indicating interaction-induced transitions. (a): Noninteracting case, where the two-photon process consists of a core electron getting excited into the $j_{\rm eff} = 1/2$ manifold followed by a de-excitation transition from $j_{\rm eff} = 3/2$ back into the core level. This would lead to a RIXS peak at $3\lambda/2$. (b),(c),(d): Interacting case, where the local Hund's coupling leads to visible multi-particle excitations. Within perturbation theory, interactions can scatter electrons into higher energy states as depicted by the solid (green) lines for the (b) initial, (c) intermediate, and (d) final states. For $J_H < \lambda$, this would lead to 2-particle peaks near 3λ but with suppressed intensity $\sim (J_H/\lambda)^2$.

and $M^{J=3/2} = \mathbb{1} - M^{J=1/2}$. The sum over all intermediate d-states in Eq. 6 can be done, which leads to

$$\mathcal{I}_J(\omega) \equiv \sum_f \left| \hat{\epsilon}^{\mu}_{\rm out} \hat{\epsilon}^{\alpha}_{\rm in} M^J_{\nu\sigma';\beta\sigma} \langle f | d_{\mu\nu\sigma'} d^\dagger_{\alpha\beta\sigma} | g \rangle \right|^2 \times \delta(E_g - E_f + \hbar\omega). \quad (10)$$

Below, we will discuss a physical picture for the excitations, before turning to exact diagonalization results.

Note that everywhere below, we will work with the single particle spin and orbital basis states for the t_{2g} electrons. However, when interactions are absent or weak compared with SOC, we will refer to the $j_{\rm eff} = 1/2, 3/2$ eigenstates. Furthermore, the core hole state is treated separately, ignoring its intermediate state interactions which is justified in the short-lifetime limit.

III. PHYSICAL PICTURE OF EXCITATIONS

In the absence of electron-electron interactions, the RIXS process is schematically illustrated in Fig. 1(a). Here, we depict spin-orbit split t_{2g} levels, having an effective (single-particle) angular momentum states, with a low energy $j_{\rm eff} = 3/2$ quartet and a higher energy $j_{\rm eff} = 1/2$ doublet. These are split by $3\lambda/2$ where λ is the spin-orbit coupling. We consider a filling corresponding to a $5d^3$ configuration (e.g., osmates), and depict the photon-induced transitions by dashed (purple) lines. For the L_3 edge, the incoming photon excites a core electron from $2P_{3/2}$ into the higher energy $j_{\rm eff} = 1/2$ state, followed by a de-excitation from the lower energy $j_{\rm eff} = 3/2$ manifold into the core-level. Such inelastic processes would lead to only a *single* peak at $\hbar\omega = 3\lambda/2$.

Next, let us consider interactions between electrons in the t_{2g} manifold, given by

$$H_{\rm int} = \frac{U}{2} : (\sum_\ell n_\ell)^2 : -5\frac{J_H}{2} \sum_{\ell<\ell'} n_\ell n_{\ell'} - 2J_H \sum_{\ell<\ell'} \vec{S}_\ell \cdot \vec{S}_{\ell'} + J_H \sum_{\ell\neq\ell'} d^\dagger_{\ell\uparrow} d^\dagger_{\ell\downarrow} d_{\ell'\downarrow} d_{\ell'\uparrow} \quad (11)$$

with :: denoting normal ordering. Here the various terms in the Kanamori interaction are: (i) the total "charging energy" to change the electron number at a site, (ii) the difference term between interorbital and intraorbital charge repulsion, (iii) the Hund's exchange between spins in different orbitals, and (iv) singlet pair hopping between orbitals. While the first term is governed by the "Hubbard U", the latter three interactions are all set by the Hund's coupling. Since RIXS is a number conserving process, and the intermediate state of the t_{2g} orbitals plays no role in the expression in Eq. 10, the charge repulsion U plays no role in determining $\mathcal{I}_J(\omega)$. The interactions relevant to RIXS are therefore parameterized by a single energy: the Hund's coupling J_H.

Such interaction effects will lead to *multiple* peaks in the RIXS spectrum, deviating from the single-particle expectation. At the perturbative level, this stems from two reasons. First, many-body effects will split the degeneracies associated with the single-particle states; this will split the peak at $3\lambda/2$ into multiple peaks separated by the interaction energy scale J_H. Second, interactions can perturbatively excite electrons into higher energy single-particle states. This is shown in Figs. 1(b-d), where interactions excite electrons between $j_{\rm eff} = 3/2$ and $j_{\rm eff} = 1/2$ states as shown by the solid (green) line. This can happen in the ground, intermediate, or final states, and it leads to transitions into final states with *two* electrons excited across the spin-orbit gap. Such 'multi-particle' excitations will produce a second set of peaks around an

energy $\sim 3\lambda$. For small J_H/λ, these secondary peaks will have an intensity $\sim (J_H/\lambda)^2$. This is in addition to any suppression of matrix elements arising from quantum numbers (i.e., selection rules).

Below, we will use the expression in Eq. 10, and present results from a (non-perturbative) numerical computation using exact diagonalization for the g, n, f states of the t_{2g} orbitals. While we have presented preliminary results for the case of the iridates in previous work, we focus here on other fillings, which are also relevant to the osmates and rhenates.

IV. EXACT DIAGONALIZATION RESULTS

A. Mode energies

We have used the t_{2g} orbital basis with SOC and the Kanamori interaction, and numerically computed the eigenstates and the RIXS intensity from Eq. 10 using exact diagonalization. The projection to the t_{2g} levels is justified by the large crystal field splitting as seen in the ab initio results (discussed below). We consider different fillings d^2, d^3, d^4, and compare the resulting energies in the spectrum to the experimental results[54–57] for various $5d$ Mott insulating oxides: (i) Ba_2YReO_6 (d^2 rhenate), (ii) Ca_3LiOsO_6 and Ba_2YOsO_6 (d^3 osmates), and (iii) Sr_2YIrO_6, Sr_2GdIrO_6, and Ba_2YIrO_6 (d^4 iridates). A best fit of the excitation energies to previously published experimental spectra allows us to extract the SOC strength λ and the Hund's coupling J_H. The results are summarized in Table I, where we also show the excitation energies from theory and experiments. The agreement is good, showing that the projection to the t_{2g} sector yields an effective description of the RIXS data.

Material		λ	J_H	Peak 1	Peak 2	Peak 3	Peak 4
Ba_2YReO_6	Ex			*[0.40]*	*[0.50]*	*0.83*	*1.85*
(ref.55,this)	Th	0.380	0.260	0.41	0.47	0.89	1.83
Ba_2YOsO_6	Ex			*0.745*	*0.971*	*1.447*	*1.68*
(ref.54)	Th	0.335	0.275	0.75	0.91	1.46	1.71
Sr_2YIrO_6	Ex			*0.39*	*0.66*	*1.30*	*∼2*
(ref.55)	Th	0.425	0.250	0.41	0.64	1.31	2.06
Ba_2YIrO_6	Ex			*0.35*	*0.60*	*1.18*	-
(ref.56)	Th	0.385	0.230	0.37	0.58	1.19	1.88

TABLE I. Table showing the optimal λ, J_H (in eV) in different materials deduced from fitting the theoretical calculations to experimental RIXS excitation energies. We present the comparison of the observed (from Refs. 54–56) RIXS peak energies (in eV) (top, 'Ex', in italics) with the corresponding theoretical values (bottom, 'Th') for the optimal parameter set computed here. For Ba_2YReO_6, peaks #1 and #2 (in square brackets) were not previously resolved with L_2 edge RIXS, but are resolved here using the L_3 edge (see text and Fig. 3). For Sr_2YIrO_6, peak #4 is seen as a very weak $\sim$ 2eV feature, and it is absent in the nominally cubic Ba_2YIrO_6. Results for Ca_3LiOsO_6 (Ref. 54) and Sr_2GdIrO_6 (Ref. 55) are nearly identical to Ba_2YOsO_6 and Sr_2YIrO_6 respectively.

B. Spectral intensities

RIXS experiments are typically carried out in the 'horizontal geometry' where the in-photon polarization lies in the scattering plane, with the scattering angle to be $2\theta = 90°$, so that $\hat{\epsilon}_{\rm in} \cdot \hat{\epsilon}_{\rm out} = 0$. Fig. 2 shows the spectrum computed for this scattering geometry. Here, we average over $\hat{\epsilon}_{\rm out}$ with $\hat{\epsilon}_{\rm in} \cdot \hat{\epsilon}_{\rm out} = 0$. The precise incident polarization direction does not matter since the results are rotationally invariant (so single crystals and powder samples should yield the same result in this 'atomic limit'). We have chosen experimentally relevant values for the resolution, with a full width at half maximum (FWHM) of 100meV (rhenates, L_2 edge), 150meV (osmates, L_3 edge), and 40meV (iridates, L_3 edge). In all cases, the two lower energy peaks (energies $\lesssim$ 1eV), which, as discussed above, arise from single-particle excitations across the spin-orbit gap have higher spectral weight, while the higher energy peaks which are due to multiparticle excitations have weaker intensity. This is in reasonable agreement with experiments across all materials. The iridates, which have a non-degenerate $J_{\rm eff} = 0$ ground state are most robust to interaction effects, and exhibit negligible intensity for two-particle excitations.

C. L_3 edge RIXS for rhenates

RIXS measurements at Re L3 edge (E_i=10.537 keV) were carried out at the 27ID-B beam line at Advanced Photon Source. The same polycrystalline sample of Ba_2YReO_6 used in Ref. 51 was used. The beam was monochromatized by Si(111) double-crystal and a Si(119) channel-cut secondary crystal. A spherically diced Si(119) analyser with 2m radius of curvature was used to achieve an overall energy resolution of 60meV. A horizontal scattering geometry with scattering angle $2\theta = 90°$ was used to minimize elastic background. The measurement was carried out at room temperature. This measurement allows us to resolve the splitting between two low energy peaks at $\hbar\omega = 0.40$eV and 0.50eV, which was unresolved in previous RIXS measurements and appeared as a single peak. This data provides further quantitative confirmation of our theoretical predictions, and it is included in Table I. Note that the intensity of the highest energy 1.8eV peak, seen clearly in the published L2 edge data[55], vanishes in the L3 edge data; since the peak positions themselves do not depend on which edge is used in the RIXS, we have chosen to make the theory plot in Fig. 2 for the L2 edge for which the 1.8eV peak is also clearly visible.

D. Discussion

Our model Hamiltonian in the t_{2g} spin-orbital sector provides a good description of the RIXS data, with comparable strengths of the SOC λ and Hund's coupling J_H.

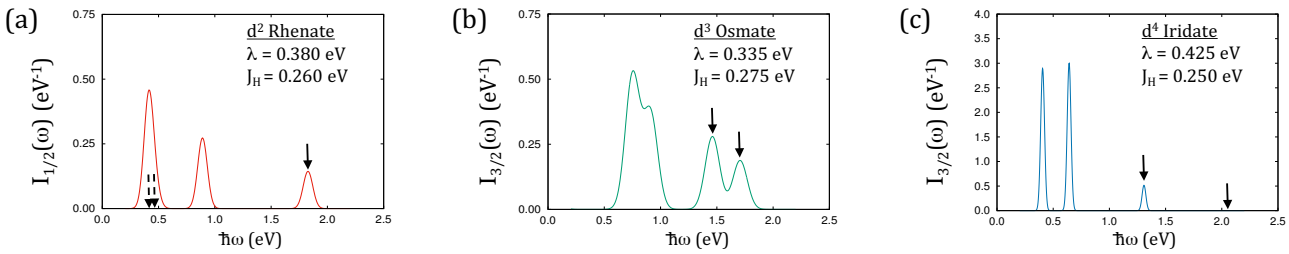

FIG. 2. (Color online) Theoretically computed RIXS spectrum for (a) d^2 rhenates (L_2 edge), (b) d^3 osmates (L_3 edge), and (c) d^4 iridates (L_3 edge) broadened by instrumental resolution. We have used shown best fit values for λ (SOC) and J_H (Hund's coupling). In (a), dashed arrows indicate two closely spaced peaks, which are not resolved in L_2 edge RIXS; see Fig. 3 for new L_3 edge RIXS which detects this splitting. In all panels, solid arrows indicate 'two-particle' transitions due to Hund's coupling.

Thus, the site-localized limit provides a good starting point to understand these double perovskites. However, a strict projection of the physics to t_{2g} orbitals completely ignores the e_g states. Furthermore, the d-orbitals of the transition metal ions are expected to hybridize with the neighboring oxygens. Such effects could be important in relating the t_{2g} model Hamiltonian parameters to a more microscopic description.

For instance, Table I shows a small, but systematic, difference between the RIXS peak energies in polycrystalline cubic Ba_2YIrO_6 from Ref. 56, and those reported on single crystals of Sr_2YIrO_6 and Sr_2GdIrO_6 in Ref. 55. This must be attributed to the different size of Ba ion compared with Sr, which leads to slight differences in bond lengths and angles of the IrO_6 octahedra, suggesting that Ir-O hybridization might lead to renormalization of λ and J_H. Table I also shows that the inferred SOC λ for Os is smaller than both Re and Ir, while the corresponding Hund's coupling is slightly larger. Again, such a non-monotonic trend across the 5d series reflects how the two microscopic effects discussed above might renormalize the parameters of the effective Hamiltonian. Such effects may be phenomenologically accounted for by going beyond the Kanamori Hamiltonian, for instance by modifying the coupling strengths appearing in Eq. 11 as done in Ref. 54 for the osmates. Below, we use electronic structure calculations to provide an *ab initio* perspective.

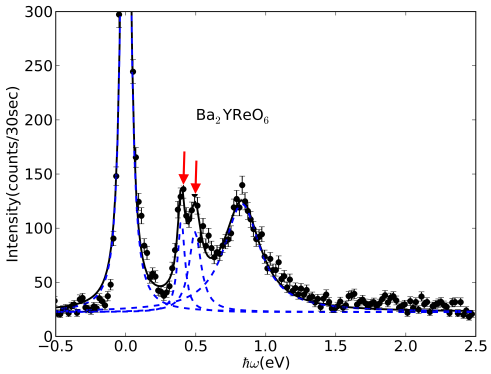

FIG. 3. (Color online) RIXS intensity as a function of energy transfer $\hbar\omega$ in Ba_2YReO_6. The RIXS spectrum was obtained near Re L_3 edge with incident energy, E_i = 10.537keV. A scattering geometry with 2θ=90° was used to minimize elastic background. The two indicated peaks at $\hbar\omega$ = 0.40eV and 0.50eV were unresolved in previous L_2 edge measurements.

V. AB INITIO ELECTRONIC STRUCTURE CALCULATIONS

We carried out density functional theory (DFT) calculations for the cubic double perovskites Ba_2YReO_6, Ba_2YOsO_6, and Ba_2YIrO_6. From a structural viewpoint, these cubic double perovskites can be regarded as consisting of clusters of the metal atom $\mathcal{M}$ with the six O ions comprising the $(\mathcal{M}O_6)^{7-}$ octahedral cage, separated by Ba and Y ions that maintain the charge balance. We used the generalized gradient approximation (GGA) of Perdew, Burke and Ernzerhof (PBE)[58], with the addition of an on-site Coulomb repulsion using the PBE+U method (U= 4 eV) in the so-called fully localized limit, and the general potential linearized augmented planewave (LAPW) method[59] as implemented in the WIEN2k code.[60] In this method U is a parameter applied in order to mimic the effects of Coulomb correlations[61]. This value is applied in the LAPW method to the d-orbitals within an LAPW sphere. Typical values for transition metal oxides range from 4 eV to 8 eV. In the present case, where we deal with a multi-orbital 5d material, low values are likely to be more physical. We find that 3 eV is inadequate to give an insulating gap for all the compounds studied, while experimental resistivity data suggests insulating character. We choose 4 eV because this is adequate to give an insulating gap in all compounds at least for an AFM state. Further details of the DFT calculations are given in Appendix A. Note that in our *ab initio* electronic structure calculations, we rely on experimental lattice parameters to fix atomic positions because they are well established for these materials and are without doubt more accurate than can be obtained from DFT.

For all three materials, we have studied $5d$ moments arranged in a type-I antiferromagnetic (AFM-I) pattern and a ferromagnetic (FM) pattern. The calculated DOS for FM order in different compounds are given in the Appendix. For FM order, the DOS peaks are generally broader, leading to incomplete gapping for the Ir and Re compounds. We also considered non-spin-polarized solutions which, however, are not energetically favored for any of the compounds studied even with U = 0 eV. This argues against explanations for the lack of observed magnetic ordering in the Ir and Re compounds that rely on the absence of moments.

A. Crystal field splitting

Fig. 6 shows the metal d projection of the calculated density of states (DOS) for all three compounds, including the spin projections, in the AFM-I state. We see that all compounds show a very large crystal field splitting, with t_{2g} states, which are near the Fermi energy ($E = 0$), being well separated from the e_g-like states at $\approx \pm 5$eV. These e_g-like states correspond to strongly hybridized bonding and anti-bonding combinations of $5d$ e_g states and O $2p$ states arising from a significant σ-overlap. This large crystal-field splitting is consistent with RIXS data.[54–56] Since the top of the t_{2g} DOS is separated from the bottom of the e_g-like DOS by $\approx$ 2eV, a model based on just the t_{2g} orbitals, as we have discussed above, is appropriate to understand the RIXS spectra for energy transfers $\hbar\omega \lesssim$ 2eV in all the compounds. However, as we discuss next, a detailed examination of the spin and charge distribution within the $(\mathcal{M}O_6)^{7-}$ cluster, and a study of different magnetic ordering patterns, reveals interesting physics beyond the atomic limit.

B. Spin and orbital moments

For U = 4eV, we find that all three compounds are insulating and show local moment behavior in the sense that the spin and orbital moments on the metal site are practically identical for the AFM and FM orders. A summary of the moments is given in Table II.

We start with a discussion of the spin-moment. As seen from the values of M_{spin}, the total spin in the unit cell in the FM pattern, SOC only weakly reduces the total spin-moments from the nominal values of 2 μ_B/atom for Re and Ir, and 3 μ_B for Os (based on electron count in an isolated t_{2g} shell). However, the moments as quantified by the part residing in the metal sphere, m_{spin}, are only $\approx$2/3 of the total moment, with the strongest reduction (to $\sim$60%) for the Ir case. This deficit is because some of the moment in the $(\mathcal{M}O_6)^{7-}$ cluster is on the O site. (Within our DFT calculations for Ba_2YIrO_6, decreasing U leads to moment reduction on the Ir site, which may bring it in closer alignment with susceptibility measurements. However, we find that this also leads to a metallic DOS, in apparent contradiction with transport data. We return to this issue later.)

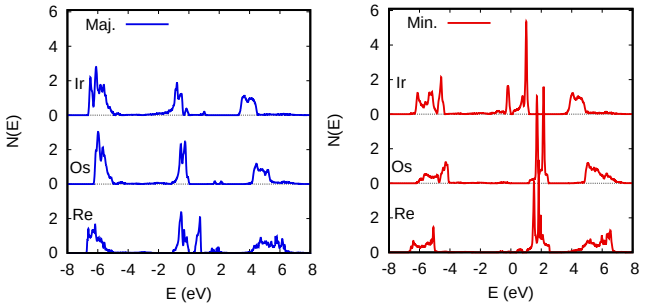

FIG. 4. (Color online) $5d$ projections of the electronic density of states onto the Ir, Os, and Re LAPW spheres of majority and minority spin character on a per ion basis. The Os values are offset and the energy zero is at the highest occupied state.

It is also interesting to note that while the Re and Os compounds have orbital moments in accord with the *ionic* Hund's rule (i.e., opposite to the spin moment), this is not the case for the Ir compound. This is a consequence of the strong crystal field splitting noted above, between the t_{2g} and e_g orbitals. This reversal of the orbital moment for the Ir compound does not follow the third Hund's rule for a free ion, but does follow the Hund's rule if one considers the t_{2g} orbital as an independent shell (i.e. as an effective p level, which is now more than half full for the Ir compound).

Finally, we turn to the issue of why DFT finds large induced O moments in these compounds. The explanation lies in an indirect exchange mechanism where the on-site Hunds exchange coupling couples the t_{2g} moments to produce an exchange splitting of the e_g $5d$ orbitals, which occur both in the e_g upper crystal field level and at the bottom of the O $2p$ bands as seen from Fig. 6. This leads to the spin dependent hybridization of the e_g orbitals, and therefore a magnetization of the nominally O $2p$ derived bands.

We note that the LAPW method divides space into non-overlapping spheres centered at the atoms and a remaining interstitial space. The O spheres in our calculation are necessarily small due to this non-overlapping requirement, and therefore the moment in these spheres underestimates the O contributions, but is expected to be roughly proportional to them. The contribution from the LAPW spheres of the six O around a given transition metal atom are 0.20μ_B, 0.47μ_B, and 0.44μ_B, for the Re, Os and Ir compounds, respectively. Note that the total of the O and transition metal atoms is not the total moment due to the interstitial, and also that even with a gap, the spin-orbit interaction reduces the total spin moments from nominal integer values that may be expected from the band filling.

TABLE II. Calculated spin and orbital moments m (in μ_B) in the transition metal LAPW sphere for AFM and FM arrangements (see text) from DFT calculations with U=4 eV. M_{spin} is the total spin moment per formula unit including all atoms for the FM case. $\Delta E = E_{FM} - E_{AFM}$ is the energy difference (per formula unit) between FM and AFM states.

Material	AFM		FM			ΔE
	m_{spin}	m_{orb}	m_{spin}	m_{orb}	M_{spin}	(meV)
Ba_2YReO_6	1.27	-0.59	1.30	-0.66	1.97	3.6
Ba_2YOsO_6	1.87	-0.12	1.89	-0.13	2.95	54.5
Ba_2YIrO_6	1.09	+0.40	1.09	+0.39	1.87	0.4

C. Magnetic ordering

Our DFT calculations yield magnetic ground states in all three compounds, in that the AFM-I structure gives lower energy than a non-magnetic case. This result is robust against changes in the parameter U, and in particular also holds for U=0. However, we find that the exchange interaction between $(\mathcal{M}O_6)^{7-}$ clusters, as quantified by the AFM-FM energy difference, while always antiferromagnetic, is one to two orders of magnitude smaller in the Re and Ir compounds as compared to the Os compound. This may be important for explaining experiments showing evidence for the presence of moments in the Ir and Re compounds, but without the robust long range order observed in the Os compound.

For Ba_2YOsO_6, the magnetic structure has been experimentally determined[62] to be type-I AFM order below a Néel temperature $T_N = 69$K. Indeed our results show that AFM-I order leads to a lower energy than FM order. Based on the energy difference $\Delta E = E_{FM} - E_{AFM} = 54.5$meV per Os, we infer a high Curie-Weiss temperature $\Theta_{CW} \gtrsim 600$K, consistent with experiments.[62]

For Ba_2YReO_6, we find a much smaller energy difference $\Delta E = 3.6$meV, so that we expect magnetic ordering tendencies are much weaker. Experimentally, Ba_2YReO_6 is reported to show a glassy magnetic ground state possibly without long range order and without evidence in thermodynamics or susceptibility for a fluctuating state.[63–65] We suppose that an AFM-I state may be the true ground state if a perfectly chemically ordered sample could be made, with the observed glassy state resulting from low levels of disorder. Oxygen vacancies if present in large quantities might also provide a source of disorder affecting ordering.

The results on Ba_2YIrO_6 are still controversial,[56,57,66–70] with experimental reports of magnetism being attributed to impurities or to weakly fluctuating $\sim 0.4\mu_B$ moments whose origin is unclear. Previous electronic structure calculations and model studies[26,28,66,68,71] reach somewhat contradictory conclusions based on whether one starts from a band picture or an atomic picture. From our calculations with $U = 4$eV, we find a significant moment $\sim 1.5\mu_B$ on the $(IrO_6)^{7-}$ cluster, but with $\Delta E = 0.4$meV which would imply a negligibly small exchange coupling between moments on neighboring clusters. The value of the energy difference is sensitive to the parameter U, but we verified that it remains much smaller than in the Os compound for different values. At some values of U (e.g. $U = 3$eV) the ferromagnetic order can even have lower energy than the AF-I order. Assuming that the experimentally measured moments in Ba_2YIrO_6 are indeed intrinsic, our calculations could help to understand why these moments may not order down to very low temperatures.

We note that the very small energy difference between ferromagnetic and antiferromagnetic orderings means that the inter-site exchange couplings are small, which is the reason for inferring weak magnetic interactions. As noted previously[72,73], in 4d and 5d double perovskites, oxygen takes a substantial spin polarization leading to effective MO_6 octahedral magnetic clusters. These interact through the O atoms so that the contact and distances between O in different octahedra is important for the exchange. This suggests a sensitivity to structure. It will be of interest to experimentally explore strain and pressure effects on magnetic order in these compounds especially to better understand the non-ordered states of the Re and Ir compounds; this is a topic for future investigation.

VI. DISCUSSION

Our ED results show that the RIXS excitations in all the $5d$ double perovskites are well described by the atomic limit picture. In this limit, the d^2 rhenates and d^3 osmates should support local moments, which is consistent with our complementary electronic structure calculations. In addition, our *ab initio* estimates for the exchange interaction strength is consistent with experiments which find robust magnetic order in Ba_2YOsO_6 as opposed to Ba_2YReO_6. However, the ED and DFT calculations are in disagreement for the ground state of Ba_2YIrO_6. While the atomic limit ground state in ED is a $J_{\text{eff}} = 0$ singlet, our DFT results indicate that the d^4 iridates should show a significant local moment in the insulating phase.

Within our DFT calculations on Ba_2YIrO_6, we find that decreasing U leads to a smaller moment on the Ir site. This could partially bridge the gap with ED, and may bring the moment in closer alignment to that inferred from susceptibility measurements,[66,67] However, the resulting state then becomes metallic which seems to be at odds with the apparently insulating resistivity,[68] unless we ascribe this to disorder induced localization. Assuming that the insulating transport is intrinsic and due to interactions, we are led to conclude that quantum spin-orbital fluctuations and dynamical self-energy effects beyond DFT must be crucial in Ba_2YIrO_6. Including these may lead to one of two outcomes. (i) This could stabilize a Mott insulator with small moments which are weakly coupled, which could explain both the

susceptibility and transport data, showing that going beyond the simple atomic limit is important. (ii) Alternatively, it might stabilize the $J_{\rm eff} = 0$ state as in our ED study; the measured magnetism must then be attributed to defects.[68,70]

At the same time, in order to understand potentially how the atomic limit picture might weakly break down in Ba_2YIrO_6, it is useful to study an isolated IrO_6 octahedral cluster which allows for some degree of electron delocalization in the Mott insulating phase. Within a perfect octahedral cage, the e_g orbitals of Ir will each hybridize with one appropriate symmetry combination of the p_σ oxygen orbitals. Similarly, each t_{2g} orbital can hybridize with only one symmetry combination of the p_π orbitals. Figs. 5(a),(b) present an illustrative level scheme where we have shown how the σ-hybridization leads to Ir-O e_g levels which are strongly split, while the smaller π-hybridization of the t_{2g} states with a subset of O p_π, leaving a residual set of non-bonded O levels. For hybridized states, we have used the notation Ir-O and O-Ir to respectively depict states which are dominantly Ir versus dominantly O. Here, the numbers indicate the level degeneracy (including spin). Incorporating SOC, as shown in Fig. 5(c), leads to hybridized $j_{\rm eff} = 1/2, 3/2$ states. Based on this final level scheme, all states upto and including Ir-O $j_{\rm eff} = 3/2$ are filled, while the Ir-O $j_{\rm eff} = 1/2$ and antibonding Ir-O e_g states are unfilled, leading to a $J_{\rm eff} = 0$ ground state. This level scheme is consistent with the 'atomic' limit, with the effective SOC, as determined from the separation between the Ir-O $j_{\rm eff} = 3/2$ and $1/2$ states, being set by the atomic SOC and the degree of Ir-O hybridization.

If Ba_2YIrO_6 is a Slater insulator with AFM order, electron itinerancy is expected to lead to a mixing of the $j_{\rm eff} = 1/2, 3/2$ levels in forming bands. However, as discussed earlier, it is unclear if this picture holds, since the charge gap $\gtrsim$ 100meV inferred from transport measurements is much larger than the tiny energy scale (few Kelvin) for magnetism.[68] On the other hand, if Ba_2YIrO_6 is a Mott insulator, with the weak moments found in experiments indeed being intrinsic, it is clear that the tiny Ir-Ir superexchange, which is far smaller than SOC, cannot destabilize the $J_{\rm eff} = 0$ singlet and lead to these moments. So the 'exciton condensation' mechanism for $J_{\rm eff} = 0$ Mott insulators studied in Refs. 22 and 24 cannot be operative here. However, the origin of the moments could arise from Ir-O interactions within an IrO_6 cluster. In this case, our level scheme suggests some potential intrinsic mechanisms to explain the magnetic moments reported in the Mott insulator. For instance, electron interactions might lead to a partial depletion of the non-bonded O levels just below the Fermi level and partial occupation of the $j_{\rm eff} = 1/2$ Ir-O level. This is one way in which going beyond the atomic limit in the ED calculations might lead to a breakdown of the strict $J_{\rm eff} = 0$ picture for the Mott insulator, resulting in the formation of weak moments. This state may be schematically represented as $|{\rm Ir}^{5+}\rangle|{\rm O_{nb}\ no-hole}\rangle + \epsilon|{\rm Ir}^{4+}\rangle|{\rm O_{nb}\ 1-hole}\rangle$,

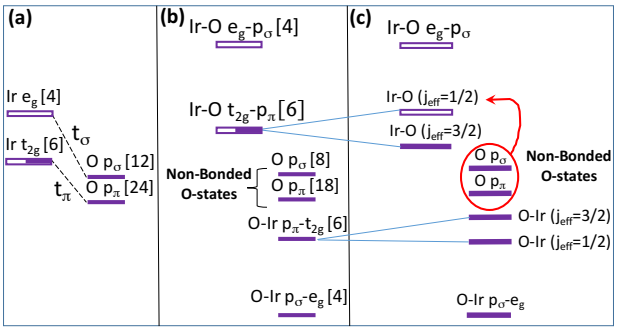

FIG. 5. (Color online) Schematic single-particle level diagram for Ir and O orbitals in the IrO_6 cluster of Ba_2YIrO_6, with filled, partially filled, and empty boxes indicating electron filling. (a) Ir and O orbitals showing small crystal field splitting in the absence of hybridization; dashed black lines show inter-site hybridization via hopping matrix elements t_σ, t_π. Numbers indicate degeneracies of the orbitals including spin. (b) Hybridization leads to a large splitting of the σ-hybridized orbitals, and to a smaller splitting of the π-hybridized orbitals, together with a set of unbonded O orbitals. The notation Ir-O or O-Ir indicates respectively that the Ir or O states are the dominant contribution to the hybridized wavefunction. (c) SOC (thin blue lines) on Ir leads to a splitting of the hybridized Ir-O and O-Ir t_{2g} states. Nominally filled and unfilled levels are indicated by filled and empty boxes in this final schematic, which would lead to a $J_{\rm eff} = 0$ insulator. Arrows shows possible impact of interactions which might cause a partial occupancy of the $j_{\rm eff} = 1/2$ hybridized Ir-O level; such "intracluster excitons" may lead to a Mott insulator with weak magnetic moments.

where 'O_{nb}' denotes non-bonded oxygen orbitals. Alternatively, interactions which generalize the rotationally invariant Kanamori form may lead to mixing of the form $|J_{\rm eff} = 0\rangle + \epsilon|J_{\rm eff} = 1\rangle$ on the Ir site since the Ir-O wavefunctions are not strictly ionic but represent states hybridized with oxygen. In analogy with previous work,[22,24] we may term such states as 'intracluster excitons'. Such excitons would be dispersionless, with extremely weak coupling between clusters leading to possible weak long-range magnetic order. Further studies of such a cluster Hamiltonian would be valuable in exploring this scenario, since it is unclear if these intrinsic explanations for the observed moments can also simultaneously be as successful at describing the RIXS data as our present model.

VII. SUMMARY

We have shown that the theory of RIXS yields mode energies and spectral intensities for $5d$ complex oxides at different fillings which are in good agreement with experiments, leading to estimates of SOC and Hund's coupling. Our work provides a natural interpretation of the low energy peaks as single-particle excitations across the spin-

orbit gap, which are split by Hund's interaction, and the higher energy peaks as emerging from two-particle excitations across the spin-orbit gap which also leads to a lower intensity. We note that recent work on $4d$ and $5d$ oxides suggests that t_{2g}-e_g interactions might become important for certain parameter regimes,[27] thus going beyond the approximation of projecting to the t_{2g} orbitals. Our *ab initio* calculations show that the e_g states might also enter the picture differently, via strong hybridization with ligand oxygens. Our electronic structure calculations allow us to extract the exchange interactions, from which we deduce that Ba_2YOsO_6 should show robust AFM ordering, but that Ba_2YReO_6 and Ba_2YIrO_6 have very weak exchange interactions which would strongly suppress magnetic ordering. Finally, our electronic structure and atomic ED calculations lead us to a model for the $\mathcal{M}O_6$ cluster which may suggest a distinct mechanism for generating intrinsic weak magnetic moments in Ba_2YIrO_6.

AP, BY, and YJ were supported by the Natural Sciences and Engineering Research Council of Canada. ADC was supported by the U.S. DOE, Office of Science, Basic Energy Sciences, Materials Sciences and Engineering Division

* arunp@physics.utoronto.ca
† singhdj@missouri.edu

[1] W. Witczak-Krempa, G. Chen, Y. B. Kim, and L. Balents, *Annual Review of Condensed Matter Physics*, Annual Review of Condensed Matter Physics **5**, 57 (2014).
[2] B. J. Kim, H. Jin, S. J. Moon, J.-Y. Kim, B.-G. Park, C. S. Leem, J. Yu, T. W. Noh, C. Kim, S.-J. Oh, J.-H. Park, V. Durairaj, G. Cao, and E. Rotenberg, Phys. Rev. Lett. **101**, 076402 (2008).
[3] Y. Singh, S. Manni, J. Reuther, T. Berlijn, R. Thomale, W. Ku, S. Trebst, and P. Gegenwart, Phys. Rev. Lett. **108**, 127203 (2012).
[4] H. Gretarsson, J. P. Clancy, Y. Singh, P. Gegenwart, J. P. Hill, J. Kim, M. H. Upton, A. H. Said, D. Casa, T. Gog, and Y.-J. Kim, Phys. Rev. B **87**, 220407 (2013).
[5] K. A. Modic, T. E. Smidt, I. Kimchi, N. P. Breznay, A. Biffin, S. Choi, R. D. Johnson, R. Coldea, P. Watkins-Curry, G. T. McCandless, J. Y. Chan, F. Gandara, Z. Islam, A. Vishwanath, A. Shekhter, R. D. McDonald, and J. G. Analytis, Nat. Comm. **5**, 4203 (2014).
[6] S. H. Chun, J.-W. Kim, J. Kim, H. Zheng, C. C. Stoumpos, C. D. Malliakas, J. F. Mitchell, K. Mehlawat, Y. Singh, Y. Choi, T. Gog, A. Al-Zein, M. M. Sala, M. Krisch, J. Chaloupka, G. Jackeli, G. Khaliullin, and B. J. Kim, Nat Phys **11**, 462 (2015).
[7] T. Takayama, A. Kato, R. Dinnebier, J. Nuss, H. Kono, L. S. I. Veiga, G. Fabbris, D. Haskel, and H. Takagi, Phys. Rev. Lett. **114**, 077202 (2015).
[8] A. Biffin, R. D. Johnson, I. Kimchi, R. Morris, A. Bombardi, J. G. Analytis, A. Vishwanath, and R. Coldea, Phys. Rev. Lett. **113**, 197201 (2014).
[9] G. Jackeli and G. Khaliullin, Phys. Rev. Lett. **102**, 017205 (2009).
[10] J. c. v. Chaloupka, G. Jackeli, and G. Khaliullin, Phys. Rev. Lett. **105**, 027204 (2010).
[11] K. Foyevtsova, H. O. Jeschke, I. I. Mazin, D. I. Khomskii, and R. Valentí, Phys. Rev. B **88**, 035107 (2013).
[12] I. Kimchi, R. Coldea, and A. Vishwanath, Phys. Rev. B **91**, 245134 (2015).
[13] J. G. Rau, E. K.-H. Lee, and H.-Y. Kee, Phys. Rev. Lett. **112**, 077204 (2014).
[14] J. Reuther, R. Thomale, and S. Rachel, Phys. Rev. B **90**, 100405 (2014).
[15] K. W. Plumb, J. P. Clancy, L. J. Sandilands, V. V. Shankar, Y. F. Hu, K. S. Burch, H.-Y. Kee, and Y.-J. Kim, Phys. Rev. B **90**, 041112 (2014).
[16] I. Rousochatzakis, J. Reuther, R. Thomale, S. Rachel, and N. B. Perkins, Phys. Rev. X **5**, 041035 (2015).
[17] Y. Chen, Y.-M. Lu, and H.-Y. Kee, Nature Communications **6**, 6593 EP (2015).
[18] S. M. Winter, Y. Li, H. O. Jeschke, and R. Valentí, Phys. Rev. B **93**, 214431 (2016).
[19] M. Laubach, J. Reuther, R. Thomale, and S. Rachel, Phys. Rev. B **96**, 121110 (2017).
[20] G. Chen, R. Pereira, and L. Balents, Phys. Rev. B **82**, 174440 (2010).
[21] G. Chen and L. Balents, Phys. Rev. B **84**, 094420 (2011).
[22] G. Khaliullin, Phys. Rev. Lett. **111**, 197201 (2013).
[23] A. Akbari and G. Khaliullin, Phys. Rev. B **90**, 035137 (2014).
[24] O. N. Meetei, W. S. Cole, M. Randeria, and N. Trivedi, Phys. Rev. B **91**, 054412 (2015).
[25] J. c. v. Chaloupka and G. Khaliullin, Phys. Rev. Lett. **116**, 017203 (2016).
[26] C. Svoboda, M. Randeria, and N. Trivedi, Phys. Rev. B **95**, 014409 (2017).
[27] G. L. Stamokostas and G. A. Fiete, ArXiv e-prints (2017), arXiv:1711.02328 [cond-mat.str-el].
[28] H. Gong, K. Kim, B. H. Kim, B. Kim, J. Kim, and B. Min, Journal of Magnetism and Magnetic Materials **454**, 66 (2018).
[29] Y. J. Kim, J. P. Hill, C. A. Burns, S. Wakimoto, R. J. Birgeneau, D. Casa, T. Gog, and C. T. Venkataraman, Phys. Rev. Lett. **89**, 177003 (2002).
[30] S. Grenier, J. P. Hill, V. Kiryukhin, W. Ku, Y.-J. Kim, K. J. Thomas, S.-W. Cheong, Y. Tokura, Y. Tomioka, D. Casa, and T. Gog, Phys. Rev. Lett. **94**, 047203 (2005).
[31] D. S. Ellis, J. Kim, J. P. Hill, S. Wakimoto, R. J. Birgeneau, Y. Shvyd'ko, D. Casa, T. Gog, K. Ishii, K. Ikeuchi, A. Paramekanti, and Y.-J. Kim, Phys. Rev. B **81**, 085124 (2010).
[32] J. Kim, D. Casa, M. H. Upton, T. Gog, Y.-J. Kim, J. F. Mitchell, M. van Veenendaal, M. Daghofer, J. van den Brink, G. Khaliullin, and B. J. Kim, Phys. Rev. Lett. **108**, 177003 (2012).
[33] M. P. M. Dean, A. J. A. James, R. S. Springell, X. Liu, C. Monney, K. J. Zhou, R. M. Konik, J. S. Wen, Z. J. Xu, G. D. Gu, V. N. Strocov, T. Schmitt, and J. P. Hill, Phys. Rev. Lett. **110**, 147001 (2013).
[34] H. Gretarsson, J. P. Clancy, Y. Singh, P. Gegenwart, J. P. Hill, J. Kim, M. H. Upton, A. H. Said, D. Casa, T. Gog, and Y.-J. Kim, Phys. Rev. B **87**, 220407 (2013).

[35] M. Moretti Sala, M. Rossi, S. Boseggia, J. Akimitsu, N. B. Brookes, M. Isobe, M. Minola, H. Okabe, H. M. Rønnow, L. Simonelli, D. F. McMorrow, and G. Monaco, Phys. Rev. B **89**, 121101 (2014).
[36] S. Calder, J. G. Vale, N. A. Bogdanov, X. Liu, C. Donnerer, M. H. Upton, D. Casa, A. H. Said, M. D. Lumsden, Z. Zhao, J. Q. Yan, D. Mandrus, S. Nishimoto, J. van den Brink, J. P. Hill, D. F. McMorrow, and A. D. Christianson, Nature Communications **7**, 11651 EP (2016).
[37] J. van den Brink and M. van Veenendaal, Journal of Physics and Chemistry of Solids **66**, 2145 (2005), 5th International Conference on Inelastic X-ray Scattering (IXS 2004).
[38] J. van den Brink and M. van Veenendaal, EPL (Europhysics Letters) **73**, 121 (2006).
[39] L. J. P. Ament, F. Forte, and J. van den Brink, Phys. Rev. B **75**, 115118 (2007).
[40] J. van den Brink, EPL (Europhysics Letters) **80**, 47003 (2007).
[41] F. Forte, L. J. P. Ament, and J. van den Brink, Phys. Rev. B **77**, 134428 (2008).
[42] L. J. P. Ament, G. Ghiringhelli, M. M. Sala, L. Braicovich, and J. van den Brink, Phys. Rev. Lett. **103**, 117003 (2009).
[43] L. J. P. Ament, G. Khaliullin, and J. van den Brink, Phys. Rev. B **84**, 020403 (2011).
[44] M. van Veenendaal, ArXiv e-prints (2011), arXiv:1106.0640 [cond-mat.str-el].
[45] P. Marra, K. Wohlfeld, and J. van den Brink, Phys. Rev. Lett. **109**, 117401 (2012).
[46] P. Marra, S. Sykora, K. Wohlfeld, and J. van den Brink, Phys. Rev. Lett. **110**, 117005 (2013).
[47] M. Moretti Sala, K. Ohgushi, A. Al-Zein, Y. Hirata, G. Monaco, and M. Krisch, Phys. Rev. Lett. **112**, 176402 (2014).
[48] G. B. Halász, N. B. Perkins, and J. van den Brink, Phys. Rev. Lett. **117**, 127203 (2016).
[49] M. Kanász-Nagy, Y. Shi, I. Klich, and E. A. Demler, Phys. Rev. B **94**, 165127 (2016).
[50] Y. Shi, D. Benjamin, E. Demler, and I. Klich, Phys. Rev. B **94**, 094516 (2016).
[51] Y. Shi, A. J. A. James, E. Demler, and I. Klich, Phys. Rev. B **96**, 155101 (2017).
[52] L. J. P. Ament, M. van Veenendaal, T. P. Devereaux, J. P. Hill, and J. van den Brink, Rev. Mod. Phys. **83**, 705 (2011).
[53] B. J. Kim and G. Khaliullin, Phys. Rev. B **96**, 085108 (2017).
[54] A. E. Taylor, S. Calder, R. Morrow, H. L. Feng, M. H. Upton, M. D. Lumsden, K. Yamaura, P. M. Woodward, and A. D. Christianson, Phys. Rev. Lett. **118**, 207202 (2017).
[55] B. Yuan, J. P. Clancy, A. M. Cook, C. M. Thompson, J. Greedan, G. Cao, B. C. Jeon, T. W. Noh, M. H. Upton, D. Casa, T. Gog, A. Paramekanti, and Y.-J. Kim, Phys. Rev. B **95**, 235114 (2017).
[56] A. Nag, S. Bhowal, M. M. Sala, A. Efimenko, F. Bert, P. K. Biswas, A. D. Hillier, M. Itoh, S. D. Kaushik, V. Siruguri, C. Meneghini, I. Dasgupta, and S. Ray, ArXiv e-prints (2017), arXiv:1707.09304 [cond-mat.mtrl-sci].
[57] M. Kusch, V. M. Katukuri, N. A. Bogdanov, B. Büchner, T. Dey, D. V. Efremov, J. E. Hamann-Borrero, B. H. Kim, M. Krisch, A. Maljuk, M. M. Sala, S. Wurmehl, G. Aslan-Cansever, M. Sturza, L. Hozoi, J. van den Brink, and J. Geck, Phys. Rev. B **97**, 064421 (2018).
[58] J. P. Perdew, K. Burke, and M. Ernzerhof, Phys. Rev. Lett. **77**, 3865 (1996).
[59] D. J. Singh and L. Nordstrom, *Planewaves Pseudopotentials and the LAPW Method, 2nd Edition* (Springer, Berlin, 2006).
[60] P. Blaha, K. Schwarz, G. Madsen, D. Kvasnicka, and J. Luitz, *WIEN2k, An Augmented Plane Wave + Local Orbitals Program for Calculating Crystal Properties* (K. Schwarz, Tech. Univ. Wien, Austria, 2001).
[61] V.I. Anisimov, F. Aryasetiawan and A.I. Lichtenstein, J. Phys.: Condens. Matter **9**, 767 (1997).
[62] E. Kermarrec, C. A. Marjerrison, C. M. Thompson, D. D. Maharaj, K. Levin, S. Kroeker, G. E. Granroth, R. Flacau, Z. Yamani, J. E. Greedan, and B. D. Gaulin, Phys. Rev. B **91**, 075133 (2015).
[63] Y. Sasaki, Y. Doi, and Y. Hinatsu, J. Mater. Chem. **12**, 2361 (2002).
[64] T. Aharen, J. E. Greedan, C. A. Bridges, A. A. Aczel, J. Rodriguez, G. MacDougall, G. M. Luke, V. K. Michaelis, S. Kroeker, C. R. Wiebe, H. Zhou, and L. M. D. Cranswick, Phys. Rev. B **81**, 064436 (2010).
[65] C. M. Thompson, J. P. Carlo, R. Flacau, T. Aharen, I. A. Leahy, J. R. Pollichemi, T. J. S. Munsoe, T. Medina, G. M. Luke, J. Munevar, S. Cheung, T. Goko, Y. J. Uemura, and J. E. Greedan, J. Phys.: Condens. Matter **26**, 306003 (2014).
[66] G. Cao, T. F. Qi, L. Li, J. Terzic, S. J. Yuan, L. E. DeLong, G. Murthy, and R. K. Kaul, Phys. Rev. Lett. **112**, 056402 (2014).
[67] T. Dey, A. Maljuk, D. V. Efremov, O. Kataeva, S. Gass, C. G. F. Blum, F. Steckel, D. Gruner, T. Ritschel, A. U. B. Wolter, J. Geck, C. Hess, K. Koepernik, J. van den Brink, S. Wurmehl, and B. Büchner, Phys. Rev. B **93**, 014434 (2016).
[68] F. Hammerath, R. Sarkar, S. Kamusella, C. Baines, H.-H. Klauss, T. Dey, A. Maljuk, S. Gaß, A. U. B. Wolter, H.-J. Grafe, S. Wurmehl, and B. Büchner, Phys. Rev. B **96**, 165108 (2017).
[69] J. Terzic, H. Zheng, F. Ye, H. D. Zhao, P. Schlottmann, L. E. De Long, S. J. Yuan, and G. Cao, Phys. Rev. B **96**, 064436 (2017).
[70] Q. Chen, C. Svoboda, Q. Zheng, B. C. Sales, D. G. Mandrus, H. D. Zhou, J.-S. Zhou, D. McComb, M. Randeria, N. Trivedi, and J.-Q. Yan, Phys. Rev. B **96**, 144423 (2017).
[71] S. Bhowal, S. Baidya, I. Dasgupta, and T. Saha-Dasgupta, Phys. Rev. B **92**, 121113 (2015).
[72] I.I. Mazin and D.J. Singh, Phys. Rev. B **56**, 2556 (1997).
[73] S. Calder, D.J. Singh, V.O. Garlea, M.D. Lumsden, Y.G. Shi, K. Yamaura and A.D. Christianson, Phys. Rev. B **96**, 184426 (2017).
[74] T. Dey, A. Maljuk, D. V. Efremov, O. Kataeva, S. Gass, C. G. F. Blum, F. Steckel, D. Gruner, T. Ritschel, A. U. B. Wolter, J. Geck, C. Hess, K. Koepernik, J. van den Brink, S. Wurmehl, and B. Büchner, Phys. Rev. B **93**, 014434 (2016).

Appendix A: Details of electronic structure calculations

The DFT calculations were carried out with the generalized gradient approximation (GGA) of Perdew, Burke and Ernzerhof (PBE)[58] and the general potential linearized augmented planewave (LAPW) method[59] as im-

plemented in the WIEN2k code.[60] The LAPW sphere radii were 2.1 bohr for Ir, Os, Re and Y, 2.5 bohr for Ba and 1.55 bohr for O. We used the standard LAPW basis set plus local orbitals for the semicore states. With the PBE GGA, including magnetism, we obtain a semiconducting gap for Ba_2YOsO_6, reflecting the exchange split t_{2g} crystal field level of this d^3 system, but we do not obtain a gap in either Ba_2YReO_6 or Ba_2YIrO_6, even with magnetic order and spin orbit coupling. Experimental data (e.g. specific heat) imply that Ba_2YReO_6 is non-metallic. Experimental data is less clear for Ba_2YIrO_6 but it is presumed to be non-metallic based on transport data. Accordingly, we show electronic structures with the PBE+U method, with the choice U=4 eV. This is sufficient to open a gap in both Ba_2YReO_6 and Ba_2YIrO_6. We find that with U=3 eV, a gap is opened in Ba_2YReO_6 but not Ba_2YIrO_6, with the assumed magnetic ordering pattern. For U=4 eV, and the assumed antiferromagnetic order we obtain gaps of 0.31 eV, 1.21 eV and 0.12 eV, for the Re, Os and Ir compounds, respectively. We note that the selected value of U is higher than that used by Bhowal et al.[71] in a prior study of Iridates, where U = 2 eV was employed. In our calculations we find that neither Ba_2YIrO_6 nor Ba_2YReO_6 is insulating for U = 2 eV. From an experimental point of view it is not fully established whether Ba_2YIrO_6 is a true insulator, but resistivity data points to such a state.

For the structure we used the experimentally determined lattice parameters, a=8.3395 Å,[64] for Ba_2YReO_6 and a=8.34383 Å, for Ba_2YOsO_6,[54] and a=8.3387 Å, for Ba_2YIrO_6.[74] We relaxed the free internal parameter associated with the O position using the PBE GGA. Since bonding and moment formation are inter-related, we allowed the formation of ferromagnet moments in these relaxations, i.e. the FM order. The resulting structures have Ba at (0.25,0.25,0.25) and (0.75,0.75,0.75), Y at (0,0,0), Re/Os at (0.5,0.5,0.5) and O at (0,0,z_O) and equivalent positions, with z_O=0.2642, 0.2639 and 0.2636 for the Re, Os and Ir compounds, respectively. We used this structure for calculating electronic and magnetic properties as discussed below. All calculations included spin-orbit coupling, except for the structure relaxation.

The majority and minority DOS for the optimal AFM state have been presented in the main text. Below, we plot the corresponding DOS for the FM state.

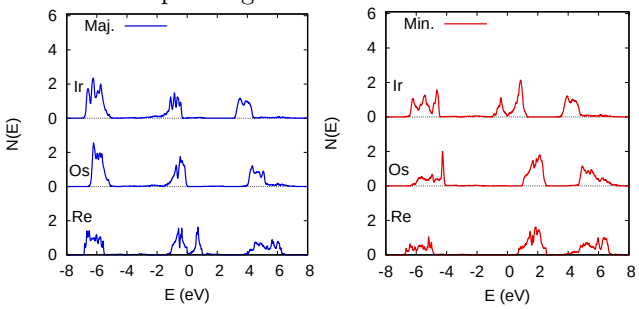

FIG. 6. (Color online) 5d projections of the electronic density of states onto the Ir, Os, and Re LAPW spheres of majority and minority spin character on a per ion basis for the FM state. The Os values are offset and the energy zero is at the highest occupied state.